J. Fluid Mech. (1990), *vol.* 210, *pp.* 329–351
Printed in Great Britain

Lunate-tail swimming propulsion. Part 2. Performance analysis

By G. KARPOUZIAN†, G. SPEDDING AND H. K. CHENG
Department of Aerospace Engineering, University of Southern California, Los Angeles, CA 90089-1191, USA

(Received 12 July 1988 and in revised form 22 August 1989)

The theory of an oscillating, high-aspect-ratio, lifting surface with a curved centreline (Cheng & Murillo 1984) is applied to a performance analysis of lunate-tail swimming propulsion. Thrust, power and propulsive efficiency are calculated for model lunate tails with various combinations of mode shapes and morphological features to ascertain the viability of the proportional-feathering concept, and to determine the influence of sweep and centreline curvature. One of the principal conclusions concerns the interchangeability of the heaving amplitude of the peduncle (identified with the major pitching axis) with the centreline sweep, and its effect on the propulsive efficiency, while maintaining the same thrust. Hydrodynamic reasons are also offered for the apparent preference for the crescent-moon fin shape over the V-shape at moderate sweep angles, and for the large sweep angles often found in V-shaped fins.

1. Introduction

Amongst the various modes of aquatic animal propulsion, the carangiform mode is characterized by the restriction of noticeable undulation to the posterior end of the body, where the caudal fin becomes primarily responsible for thrust generation. Here, the selective pressures for efficient maintenance of high-speed propulsion appear to be responsible for the convergent evolution of caudal fins of high aspect ratio. The significant morphological change typically involves the evolution towards a fin shape of the crescent-moon form, commonly referred to as the *lunate tail*, and may be identified in the only distantly related mammals (dolphins, whales), sharks, and bony fishes, as illustrated in Norman & Fraser (1937), Kramer (1960) and Lighthill (1969). Figure 1, adapted from Joseph, Klawe & Murphy (1979) shows variants of lunate-tail form among the tuna and the bill fishes. Note that at a short distance anterior to the caudal fin, where lateral oscillation amplitudes begin to rapidly increase, the body depth is greatly reduced. The practical consequence is that thrust generation is confined almost exclusively to the caudal fin, which may be considered to oscillate in an otherwise undisturbed free stream.

Lighthill (1969, 1970) gave a general survey of the hydromechanics of aquatic animal propulsion. Reasons for convergence upon the lunate tail of the thrust and propulsive efficiency were advanced, treating the lunate tail by the two-dimensional theory of oscillating airfoils in heaving and pitching modes. In this approximation, only the cross-stream components of wake vorticity were taken into account, although in reality, streamwise components must also be present; the propulsive

† Present address: United States Naval Academy, Department of Aerospace Engineering, Annapolis, MD 21402-5042, USA.

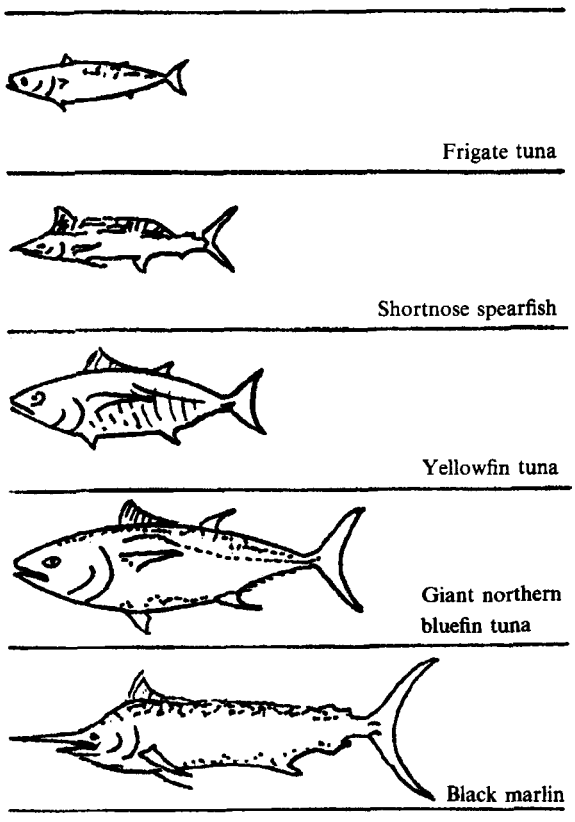

FIGURE 1. Variants of lunate-tail form among tuna and bill fishes, after Joseph *et al.* (1979).

efficiency of the lunate-tail model treated by the two-dimensional theory must therefore be an overestimate, due to an underestimation of the wake energy loss. Wu (1971*a*), for example, finds high propulsive efficiencies, close to unity (0.96–0.99) in a two-dimensional analysis. A three-dimensional analysis is clearly required for more accurate and realistic estimates of the propulsive efficiency, which, in turn, should clarify the apparent evolutionary convergence on this mechanical design.

Lunate-tail propulsion by oscillating, unyawed straight wings of high aspect ratio has been studied by Chopra (1974) and James (1975). But, as noted by Lighthill (1969), the curvature and sweep of the planform centreline might be expected to exert a strong influence on the unsteady hydrodynamics and lunate-tail performance, since the induced upwash is a functional of these parameters. Numerical calculations of thrust and propulsive efficiency of oscillating rigid flat plates as a three-dimensional lunate-tail model have been made by Chopra & Kambe (1977), applying a kernel-function method, and by Lan (1979), applying an improved doublet-lattice method. The effect of sweep on the propulsive performance remains unclear from these studies.

Noting this deficiency, the quasi-steady problem for wings with curved planform has been studied by Ashenberg & Weihs (1984) for lifting-line theory with centreline curvature, and by van Dam (1987) with a surface panel method. These works examined the wake energy loss or induced drag of planar lifting surface in the quasi-steady limit, and their results cannot directly be compared with the unsteady performance parameters presented here.

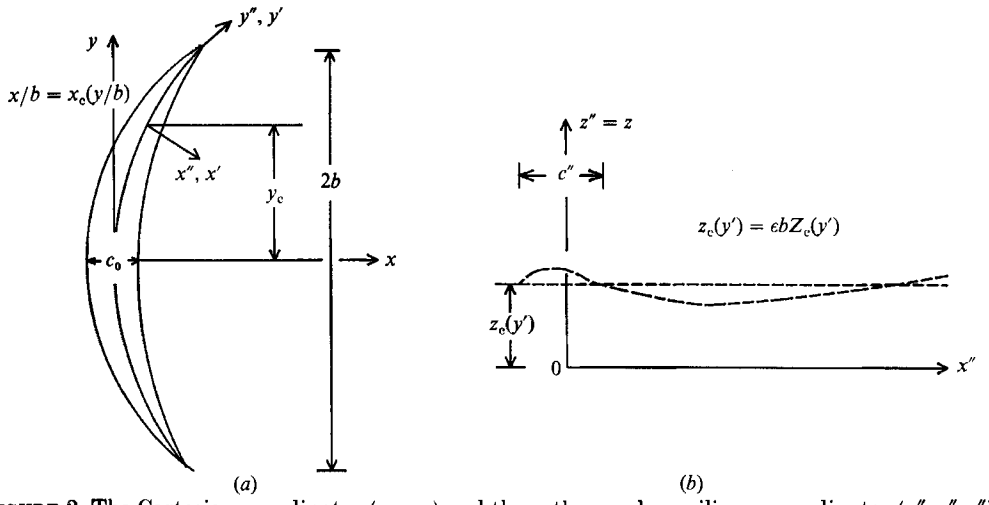

FIGURE 2. The Cartesian coordinates (x, y, z) and the orthogonal curvilinear coordinates (x'', y'', z''), the centreline of a planform, and definitions of b, c_0, c'', $x_c(y')$, z_c'' and y_c. Note that z_c is comparable with c_0 in magnitude.

Generalizing the classical lifting-line theory (Prandtl 1918; Van Dyke 1964), Cheng and Murillo (1984, hereinafter referred to as CM84) developed an asymptotic analysis of inviscid incompressible potential flow about a high aspect ratio ($A_1 \equiv 2b/c_0 \gg 1$), planar lifting surface, oscillating at a reduced frequency based on the half-span in the unit order range, i.e. $\Omega \equiv \omega b/U = O(1)$, including the quasi-steady limit $\Omega \to 0$, where b is the fin half-span, c_0 is a reference chord, ω is the circular frequency and U is the mean-stream velocity. (Fuller analytical details of this work and the problem background were documented in Cheng & Murillo's (1982) (hereinafter referred to as CM82) and in Murillo (1979).) The analysis is consistent with physiological and kinematic data reported in the literature, as summarized by Wu & Yates (1978), for example. Note that the reduced frequency based on the half-chord is small in this case, i.e. $k \equiv \omega c_0/2U \ll 1$. The analysis takes into account the centreline curvature and sweep, and is applicable to lunate-tail models provided the assumption of a planar lifting surface remains adequate. Figure 2 shows a typical planform of an isolated lunate-tail model, to which the theory is addressed. Complementary to the present work is an earlier study (Cheng 1976) for high aspect ratios at reduced frequency $k = O(1)$ and higher, i.e. $\Omega = O(A) \gg 1$.

This paper will apply and develop further the analysis of CM82 and CM84 to the performance of a lunate-tail model. Thrust, power and propulsive efficiency are calculated for model lunate tails with different combinations of mode shapes and planforms to explore the viability of the proportional-feathering concept in three dimensions, to determine the sweep-angle influence and to assess the centreline curvature effects.

2. Lighthill's theory and proportional feathering

Lighthill (1970) considers an oscillating flat plate in two dimensions, whose Cartesian ordinate z_w is

$$z_w = \mathrm{Re}\{e^{i\omega t}[h - i\alpha_L(x - x_0)]\}, \tag{1}$$

where Re signifies the real part, ω the circular frequency, and h and α_L, when taken to be real and positive, determine the amplitudes of the heaving and pitching

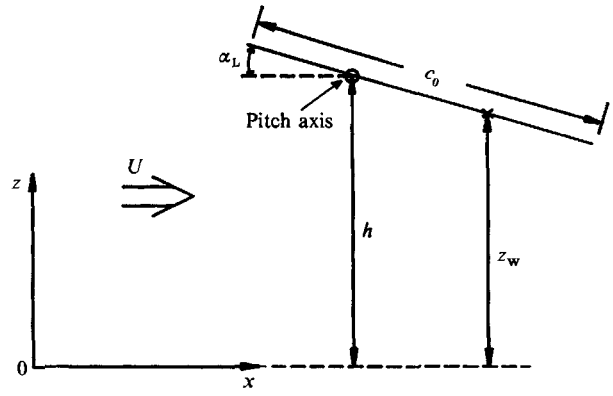

FIGURE 3. The geometric parameters of a flat plate in pitching and heaving oscillations.

oscillations, respectively. A real x_0 then gives the pitch-axis location. A pair of real h and α_L in (1) signifies a 90° phase lead of the heaving relative to the pitching, and any imaginary part in h associated with additional phase difference is equivalent to a readjustment of the pitch-axis location x_0. Figure 3 illustrates the two modes of oscillation of a flat plate in a uniform stream. The hydromechanics of this oscillating plate is controlled by three parameters: the proportional feathering parameter θ, the reduced frequency k, and the normalized pitch-axis location $\tilde{x}_0$, defined as

$$\theta \equiv \frac{\alpha_L U}{\omega h}, \quad k \equiv \frac{\omega c_0}{2U}, \quad \tilde{x}_0 \equiv \frac{x_0}{c_0}. \tag{2}$$

The important concept of proportional feathering, introduced by Lighthill (1969), characterizes the carangiform mode when the fin incidence angle α_L and the transverse (heaving) velocity $\omega h/U$ are in phase with each other. It refers to the degree to which the oscillating surface follows the trajectory of the pitch axis or, more precisely, the direction of the relative wind vector at the pitch axis.

The relative importance of the parameters in (2) is best seen from an expression of the normal surface velocity

$$\frac{\mathrm{D}}{\mathrm{D}t} z_w \equiv \left(\frac{\partial}{\partial t} + U\frac{\partial}{\partial x}\right) z_w = \mathrm{Re}\{W[\mathrm{i}(1-\theta) + 2\theta k(\tilde{x} - \tilde{x}_0)]\}, \tag{3}$$

where $\tilde{x}$ is x/c_0, and $W \equiv \omega h$ is the maximum heaving velocity at the pitch axis. If $\theta = 1$, the surface imparts no transverse disturbance to the fluid at the pitch axis; the feathering condition must be considered perfect in this case, at least at $x = x_0$. For a fixed maximum slope of the trajectory of the hinge line $\omega h/U$, the factor $(1-\theta)$ obviously determines the angle of attack (at $\tilde{x} = \tilde{x}_0$) relative to the wavy trajectory of the hinge line. Clearly, the factor $(1-\theta)$ will also control the angle of attack for the entire plate, provided the reduced frequency is sufficiently small and both θ and $\tilde{x}_0$ are finite. To maintain a fixed θ, the pitch amplitude α_L must be adjusted in proportion to the maximum slope of the trajectory $\omega h/U$, with θ entering as a constant of proportionality; hence the notion of *proportional feathering*. The definition of θ in (2) remains useful for complex h and α_L. In such a case, perfect feathering is still identified with $\theta = 1$ according to (3). The time-averaged thrust is given by

$$\langle T \rangle = \tfrac{1}{2}\pi\rho W^2 [1 - \mathrm{Re}(\theta)], \tag{4}$$

which shows that $\mathrm{Re}(\theta)$ must be less than one for useful thrust generation.

Kinematically, $\mathrm{Re}(\theta) < 1$ provides a condition assuring that the Joukowski force has a thrust component at all or most times. Lighthill (1970) has obtained an explicit analytical expression for the time-averaged values of the thrust, $\langle T \rangle$, the power required, $\langle P \rangle$, and the propulsive efficiency, $\eta \equiv U\langle T \rangle / \langle P \rangle$, for the motion. In the quasi-steady limit, the benefits of operating in a low-frequency range are most clearly exhibited by expressing the thrust and efficiency for a small $k \neq 0$, which read

$$\langle C_T' \rangle \equiv \frac{\langle T \rangle}{\frac{1}{2}\rho U^2 c_0} = 4\pi \left(\frac{h}{c} k\right)^2 (1-\theta)\,[1+\pi(1-\tfrac{1}{2}\theta)k+\ldots], \tag{5a}$$

$$\eta \equiv \frac{U\langle T \rangle}{\langle P \rangle} = 1-\tfrac{1}{2}\pi(1-\theta)k+\ldots, \tag{5b}$$

assuming for simplicity that both θ and W *are* real, and the θ and $\tilde{x}_0$ are finite. The dots represent terms of higher order in k. It is clear that the propulsive efficiency η at a low k is high, but the corresponding thrust coefficient of (5*a*), which is proportional to k^2, is low. However, the skin friction and other forms of drag may be low enough to tolerate a low $\langle C_T' \rangle$. By virtue of the factor $(1-\theta)$ in (5*b*), the high efficiency enjoyed by the slow oscillation can be further enhanced by the proportional-feathering concept when θ is close to 1. The practical significance of this observation, however, is that the reduction in thrust due to the factor $(1-\theta)$ in (5*b*) may be compensated for by raising the heaving amplitude, h/c. Note that this conclusion does not involve the pitch-axis location.

The high propulsive efficiency achievable in the two-dimensional model implies that the three-dimensional corrections may be critical in the determination of the true wake-energy loss and propulsive efficiency. Without a systematic analysis of the three-dimensional influence, it is difficult to ascertain whether the normalized wake-energy loss in the domain $\Omega = kA_1 = O(1)$ may be of order $A_1^{-2}(1-\theta)^2$, as (5*b*) would suggest. The three-dimensional study is made more important by the realization that the unsteady and three-dimensional corrections in the flow analysis are not strictly superposable, since there is a three-dimensional influence in the wake-induced effect itself (CM84). There is also the possibility of wake-energy extraction by portions of downstream panels of swept candal fin, as discussed in another context by Wu (1971*b*).

3. The lunate-tail model and proportional feathering

The surface ordinate of the model fin may be represented by two modes,

$$z_w = \mathrm{Re}\{(\epsilon b)\,e^{i\omega t}[\hat{z}_A - (x-x_A)] + (\epsilon c_0)\,e^{i\omega t}[\hat{z}_0 - \hat{\alpha}_0(y')\,(x'-x_0'(y'))]\}, \tag{6}$$

where x is the streamwise Cartesian coordinate normalized by the half-span b, x' and y' are the two orthogonal curvilinear coordinates shown in figure 4(*a*); $\hat{z}_A$ and x_A are constants, and ϵ is a small parameter which controls the magnitude of perturbations. All terms inside the two square brackets are treated as either unit-order or smaller quantities. The first mode, expressed as a linear function of the Cartesian (outer) variable x, represents the heaving and pitching motion of a rigid flat plate about the pitch axis at $x = x_A$ corresponding to the vicinity of the peduncle. The latter axis will be referred to as the major pitch axis. The second mode, expressed in the curvilinear (inner) variables x' and y', describes the heaving–pitching motion of the local fin section, with its local pitch axis set at a distance $c_0 x_0'(y')$ from the curved centreline (dash-dot curve in figure 4*a*). The constant $\hat{z}_A$ is generally complex; it determines the

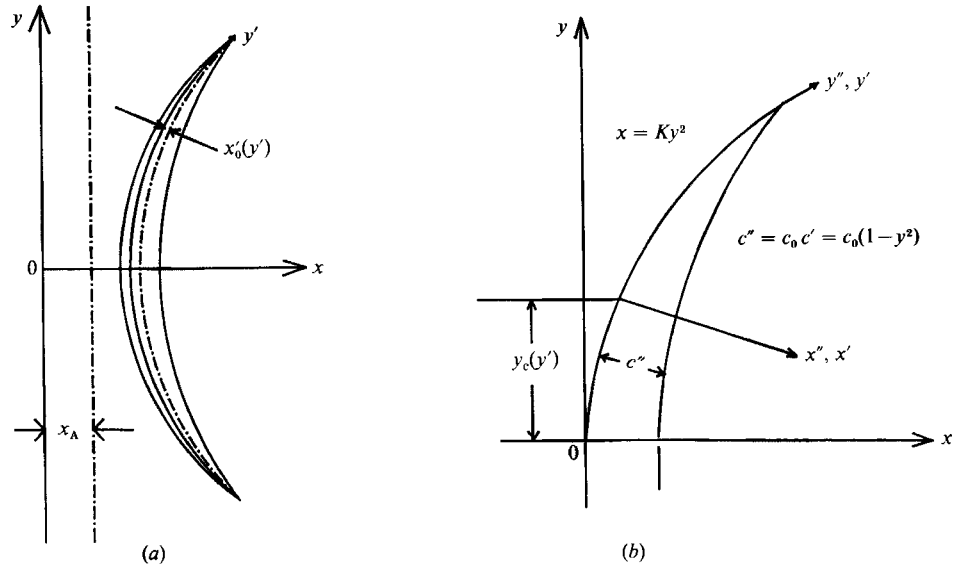

FIGURE 4. (*a*) The major pitching axis (dash-dot line) and the curved, local pitching axis (dash-dot curve) for the special class of the lunate-tail model analysed. (*b*) Planform and coordinates used in the lunate-tail model.

transverse displacement of the peduncle. A $\hat{z}_0(y') \neq 0$ would allow additional fin bending at the local hinge line $x' = x_0'$. The local pitching amplitude $\hat{\alpha}_0(y')$ may be used to account for the passive structural response of the caudal fin in twist under hydromechanical forces. A parabolic shape

$$x = Ky^2 \tag{7}$$

will be assumed for the planform leading edge and, for convenience, this will also be taken as the reference centre line $x = x_c(y)$ in the subsequent applications. To facilitate computational work, the planform trailing edge is not given in terms of x and y, but rather by the local fin chord measured normal to the y'-axis,

$$c(y') = c_0(1-y_c^2), \tag{8}$$

where y_c is a known function of y', differing slightly from y (figure 4*b*). Figure 5 illustrates the effect of varying $A_1 \equiv 2b/c_0$, the aspect ratio, and K, the average tangent of the sweep angle, on the morphology.

3.1. *Boundary condition*

The wing boundary condition may be expressed by the convective derivative of z_w. The condition can be written for an arbitrary planform in terms of the local sweep angle Λ, the frequency $\Omega \equiv kA_1$, the local pitch angle $\hat{\alpha}_0$, local pitch axis locations x_0', and also $\hat{z}_0$, as well as the important function

$$\hat{H} \equiv x_c(y') - x_A - \hat{z}_A, \tag{9a}$$

which controls the resultant heaving motion of the local fin section. A parameter corresponding to θ in (2) and (3) may be identified here as

$$\Theta \equiv \frac{\mathrm{i}(\sec\Lambda + \hat{\alpha}_0)}{\Omega\hat{H}\sec\Lambda}, \tag{9b}$$

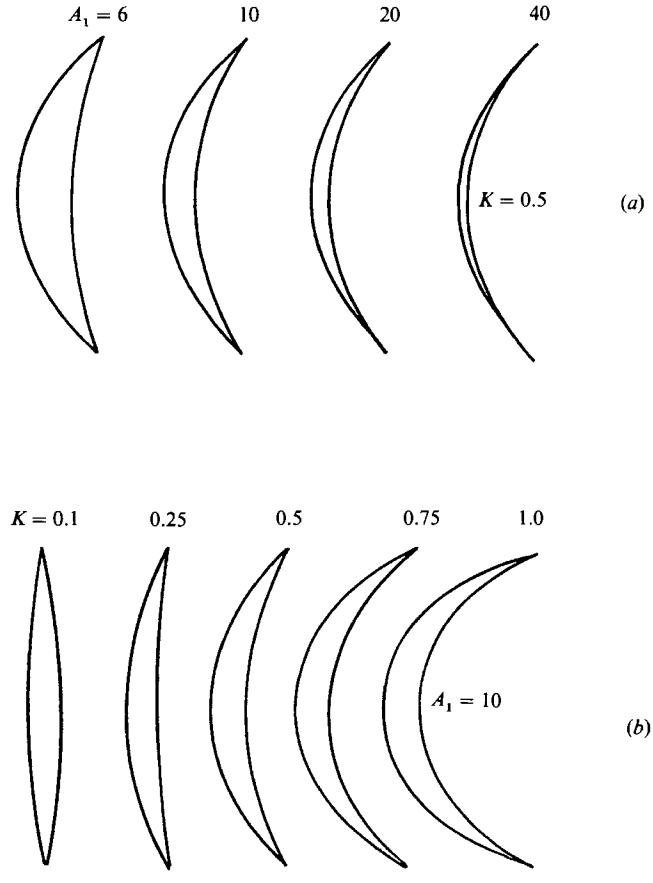

FIGURE 5. The dependence of the lunate-tail planform on (*a*) aspect ratio and (*b*) the average-sweep parameter.

which can be used to eliminate $\hat{\alpha}_0(y')$ in (6). The factor $(\sec\Lambda + \hat{\alpha}_0)$ in (9*b*) is the sum of the maximum angle of the rigid flat plate and that due to the local pitching (normalized by ϵ); the product $\Omega\hat{H}\sec\Lambda$ in (9*b*) is the maximum heaving velocity at the station y' prescribed by the rigid-plate pitching mode (normalized by $\epsilon U\cos\Lambda$). The numerator and denominator on the right-hand side of (9*b*) may thus be identified with α_L and $\omega h/U$ for the two-dimensional problem, with the additional factor of $-\epsilon$. The Θ of (9*b*) represents a localized proportional-feathering parameter corresponding to $\theta = \alpha_L U/\omega h$ in (2). Indeed, eliminating $\hat{\alpha}_0$ with Θ, the leading approximation for the transverse surface velocity (normalized by $\epsilon U\cos\Lambda$) is

$$\hat{V}^{(0)} = -\mathrm{i}\Omega\hat{H}(1-\Theta)\sec\Lambda, \tag{9c}$$

comparable to (3) for $k \to 0$. The parameter Θ thus controls the departure of $\hat{V}^{(0)}$ from its perfect feathering value, $\hat{V}^{(0)} = 0$, in our leading-order solution.

Note that h in (1) and $\hat{H}$ defined above have opposite signs. According to the discussion following (4) and (5), the condition $\mathrm{Re}\,\Theta < 1$ assures the proper incidence relative to the trajectory of the local hinge for generating a thrust component from the Joukowski lift.

The Θ considered in most examples in CM84 and the present study falls in the range $0 < \Theta < 1$; for simplicity, it will be taken to be uniform spanwise. Examples

with a fixed Θ will be referred to as the 'feathering cases'. As contrasting examples, cases with $\hat{\alpha}_0 \equiv 0$, corresponding to a rigid flat plate in oscillation, have also been studied; they will be referred to as the 'rigid cases'. It should be pointed out that, insofar as the proportional feathering is only a quasi-steady concept, an appropriate or optimum solution to the propulsion problem is expected to require a slightly non-uniform spanwise distribution of Θ. Ideally, Θ should approach unity from below for the highest propulsive efficiency, which implies, however, a vanishing thrust. For a specified thrust at levels considered below, a reasonably high efficiency may nevertheless be achieved at some $\Theta < 1$.

4. Lunate-tail propulsive performance: application of the asymptotic theory

4.1. *The time-averaged power and thrust*

The analytical base of the performance analysis is the surface distribution of the pressure jump across the lifting surface, which was examined in CM84. The symbol '$[\![\,]\!]_{\mathrm{w}}$' signifies the difference between the upper and lower surface values over the lifting surface. From the linear theory, the pressure jump is given by

$$[\![p]\!]_{\mathrm{w}} = -\rho \frac{\mathrm{D}}{\mathrm{D}t}[\![\varphi]\!]_{\mathrm{w}} = -\rho\left(\frac{\partial}{\partial t} + U\frac{\partial}{\partial x}\right)[\![\varphi]\!]_{\mathrm{w}}, \tag{10}$$

where φ is the perturbation velocity potential. The power required and the thrust generated may then be evaluated, respectively, as

$$P = -\rho \iint \frac{\mathrm{D}}{\mathrm{D}t}[\![\varphi]\!]_{\mathrm{w}} \frac{\partial z_{\mathrm{w}}}{\partial t}\,\mathrm{d}x\,\mathrm{d}y, \tag{11}$$

$$T = -\rho \iint \frac{\mathrm{D}}{\mathrm{D}t}[\![\varphi]\!]_{\mathrm{w}} \frac{\partial z_{\mathrm{w}}}{\partial x}\,\mathrm{d}x\,\mathrm{d}y + T_{\mathrm{s}}, \tag{12a}$$

where the integration extends over the entire projected lifting surface, and T_{s} is the contribution from the local leading-edge suction $T_{\mathrm{S}}^{(2\text{-D})}$:

$$T_{\mathrm{s}} = \int T_{\mathrm{S}}^{(2\text{-D})} \cos\Lambda_{\mathrm{LE}}\,\mathrm{d}y'_{\mathrm{LE}} = \int T_{\mathrm{S}}^{(2\text{-D})} \cos\Lambda_{\mathrm{LE}}\left(1 - \frac{c_0}{R}a'\right)\mathrm{d}y'. \tag{12b}$$

The line integral is to be carried out along the entire leading edge (LE), whose curvilinear coordinates are $x'' = a'' \equiv c_0 a'$. The R in (12b) is the radius of curvature of the (reference) centreline (being positive for the example illustrated in figure 2) and $\cos\Lambda_{\mathrm{LE}}$ is the cosine of the leading-edge sweep angle, related to the cosine of the centreline sweep angle $\cos\Lambda$ by

$$\cos\Lambda_{\mathrm{LE}} = \cos\Lambda - 2\frac{\sin\Lambda}{A_1}\frac{\partial a'}{\partial y'}. \tag{12c}$$

The local leading-edge suction is evaluated from the singularity of the velocity gradient in accordance with the two-dimensional theory

$$T_{\mathrm{S}}^{(2\text{-D})} = \rho\pi A^2, \tag{12d}$$

where

$$A = \lim_{x'' \to a''} \frac{\partial\varphi}{\partial x''}(x'' - a'')^{\frac{1}{2}}. \tag{12e}$$

For the sinusoidal oscillation with frequency ω, the linear system admits

$$z_{\mathrm{w}} = \mathrm{Re}(\hat{z}_{\mathrm{w}}\,\mathrm{e}^{\mathrm{i}\omega t}), \quad \varphi = \mathrm{Re}(\hat{\varphi}\,\mathrm{e}^{\mathrm{i}\omega t}), \tag{13a, b}$$

with similar expressions for other perturbation quantities, where $\hat{\varphi}$ is the solution to the reduced problem giving the frequency response. Of interest are the time-averaged values of the power and thrust, $\langle P\rangle$ and $\langle T\rangle$, which involve three time-averaged products

$$\left(\frac{\mathrm{D}}{\mathrm{D}t}[\![\varphi]\!]_{\mathrm{w}}\right)\left(\frac{\partial}{\partial t}z_{\mathrm{w}}\right),\quad \left(\frac{\mathrm{D}}{\mathrm{D}t}[\![\varphi]\!]_{\mathrm{w}}\right)\left(\frac{\partial}{\partial x}z_{\mathrm{w}}\right),\quad A^2.$$

These can be evaluated from the real parts of

$$\frac{1}{2}\frac{\mathrm{D}}{\mathrm{D}t}[\![\hat{\varphi}]\!]_{\mathrm{w}}\left(\frac{\partial}{\partial t}\hat{z}_{\mathrm{w}}\right)'',\quad \frac{1}{2}\frac{\mathrm{D}}{\mathrm{D}t}[\![\hat{\varphi}]\!]_{\mathrm{w}}\left(\frac{\partial}{\partial x}\hat{z}_{\mathrm{w}}\right)'',\quad \hat{A}\hat{A}^{**},$$

where the double asterisk signifies a complex conjugate operation.

For convenience, we introduce the power and thrust coefficients, and a coefficient for the wake-energy loss $\langle E\rangle \equiv \langle P\rangle - U\langle T\rangle$:

$$\langle \mathbb{C}_P\rangle \equiv \frac{\langle P\rangle}{\frac{1}{2}\rho U^3\epsilon^2 c_0 b},\quad \langle \mathbb{C}_T\rangle \equiv \frac{\langle T\rangle}{\frac{1}{2}\rho U^2\epsilon^2 c_0 b}, \tag{14a, b}$$

$$\langle \mathbb{C}_E\rangle \equiv \frac{\langle E\rangle}{\frac{1}{2}\rho U^3\epsilon^2 c_0 b} = \langle \mathbb{C}_p\rangle - \langle \mathbb{C}_T\rangle. \tag{14c}$$

Note that the expression for $\langle \mathbb{C}_T\rangle$ above differs from the $\langle C'_T\rangle$ of (5*a*) as the square of the magnitude of perturbation, ϵ, appears in the denominator; the coefficients defined above are generally of unit order in this theory.

4.2. *Explicit calculation of power and thrust*

The potential jump $[\![\hat{\varphi}]\!]_{\mathrm{w}}$ is determined from the jump of the coefficients in the asymptotic solution

$$\varphi' \equiv \frac{\hat{\varphi}}{\epsilon c_0 U\cos\Lambda} = \phi^{(0)} + A_1^{-1}\phi^{(10)} + k'\phi^{(01)} + \ldots, \tag{15}$$

where $k' \equiv k\sec\Lambda$. For the particular model described by (6), the jumps of

$$\partial\phi^{(0)}/\partial x', \partial\phi^{(10)}/\partial x' \quad \text{and} \quad \partial\phi^{(01)}/\partial x'$$

are given in CM82, where the functions of y' or y_{c}, $\hat{V}_0^{(10)}$, $\hat{V}_0^{(01)}$, $\hat{V}_1^{(10)}$, and $\hat{V}_1^{(01)}$ are also found. From these, $\phi^{(0)}$, $\phi^{(10)}$, and $\phi^{(01)}$, and their time derivatives may also be deduced. In particular, at each span station the circulation $\hat{\Gamma} \equiv [\![\hat{\varphi}]\!]_{\mathrm{TE}}$ (of the inner solution) can be computed from

$$\hat{\Gamma}^{(0)} = [\![\phi^{(0)}]\!]_{\mathrm{TE}} = -\pi c'\hat{V}^{(0)}, \tag{16a}$$

$$\hat{\Gamma}^{(10)} = [\![\phi^{(10)}]\!]_{\mathrm{TE}} = -\pi c'\hat{V}_0^{(10)} - \tfrac{3}{4}\pi c'\hat{V}_1^{(10)} + 2\pi c'\tan\Lambda\left(\frac{\partial}{\partial y'}(c'\hat{V}^{(0)}) + \kappa'(c'+a')\,\hat{V}^{(0)}\right), \tag{16b}$$

$$\hat{\Gamma}^{(01)} = [\![\phi^{(01)}]\!]_{\mathrm{TE}} = -\pi c'\hat{V}_0^{(01)} - \tfrac{3}{4}\pi c'\hat{V}_1^{(01)} + 2\mathrm{i}\pi c'(c'+a')\,\hat{V}^{(0)}, \tag{16c}$$

where $c' \equiv c/c_0$ is a normalized local chord, $\kappa' = -\mathrm{d}\Lambda/\mathrm{d}y'$ is a normalized centreline curvature, and the subscript TE signifies the trailing edge. The power and thrust coefficients $\langle \mathbb{C}_P\rangle$ and $\langle \mathbb{C}_T\rangle$ may each be reduced to a line integral explicit in A_1 and Ω, being functionals of y': $\hat{H}$, Θ (or $\hat{\alpha}_0$), c', and two normalized (finite parts of the) induced velocities, $\hat{V}^{\infty}_{(10)}$ and $\hat{V}^{\infty}_{(01)}$, subject to a relative error comparable with A_1^{-2}. The latter two induced velocities are themselves, however, functionals of the

centreline shape, $x = x_c(y)$, and the leading-order circulation, $\hat{\Gamma}^{(0)} = \cos\Lambda\hat{\tilde{\Gamma}}^{(0)}$, determined from the matching (CM84).

For the lunate-tail propulsion study, a slightly more general shape for the centreline than (7) has been adopted. It reads

$$x_c = Ky^2 + m_0|y| \tag{17}$$

where the second term is added to allow for V-shaped fins.

For the type of oscillation defined by (6), and the type of planforms designated by (8) and (17), the induced velocities may each be conveniently represented by a linear combination of three basic induced velocities corresponding to three normalized span loadings,

$$\hat{\Gamma} = 1-y^2, \quad \hat{\Gamma} = |y|(1-y^2), \quad \hat{\Gamma} = y^2(1-y^2), \tag{18}$$

which are independent of the mode shape constants K, m_0, x_A and $\hat{z}_A$.

The leading-order result for the power and thrust can be readily obtained from the quasi-steady strip (local two-dimensional) theory

$$\begin{aligned}\langle \mathbb{C}_P^{(0)}\rangle = \langle \mathbb{C}_T^{(0)}\rangle &= \Omega\int_{-1}^{1} \mathrm{Re}\,(\mathrm{i}\hat{H}\hat{\Gamma}_{**}^{(0)})\,\mathrm{d}y \\ &= \pi\int_{-1}^{1}\{\Omega^2|\hat{H}|^2 - \mathrm{Re}\,[\mathrm{i}\Omega(1+\hat{\alpha}_0\cos\Lambda)\,\hat{H}_{**}]\}c'\,\mathrm{d}y \\ &= \pi\Omega^2\int_{-1}^{1}|\hat{H}|^2[1-\mathrm{Re}\,(\Theta)]\,c'\,\mathrm{d}y,\end{aligned} \tag{19}$$

which is consistent with (4), and will serve as a base for subsequent discussions.

4.3. *Wake-energy loss and efficiency*

The difference $\langle P\rangle - U\langle T\rangle \equiv \langle E\rangle$, or $\langle \mathbb{C}_P\rangle - \langle \mathbb{C}_T\rangle = \langle \mathbb{C}_E\rangle$, gives the rate at which the energy is lost to the wake and is expected to be non-negative. The propulsive efficiency is

$$\eta = 1 - \frac{\langle E\rangle}{\langle P\rangle} = 1 - \frac{\langle \mathbb{C}_E\rangle}{\langle \mathbb{C}_P\rangle}. \tag{20}$$

As noted earlier, the ratio $\langle \mathbb{C}_E\rangle/\langle \mathbb{C}_P\rangle$ is anticipated to belong to the order A_1^{-1} in the domain of A_1 and k of interest. The η of (20) can be evaluated to within a relative error of $O(A_1^{-2})$. Within this degree of accuracy, it is asymptotically correct to retain only the leading-order term for $\langle \mathbb{C}_P\rangle$, i.e. $\langle \mathbb{C}_P^{(0)}\rangle$, in the calculation of η. However, in the neighbourhood where the power or thrust may approach zero (as shown in the two-dimensional analysis), or in cases where the corrections in $\langle \mathbb{C}_P\rangle$ or $\langle \mathbb{C}_T\rangle$ are relatively large (either because $(1-\Theta)$ is small, hence $\langle \mathbb{C}_T^{(0)}\rangle$ is small, or because the corrections themselves are numerically significant), a fuller expression for the power and thrust coefficients is required.

This power coefficient reads

$$\begin{aligned}\langle \mathbb{C}_P\rangle = -\frac{\pi}{K^2\Omega^2}\int_{\mathrm{span}} c'\cos^2\Lambda\,\mathrm{Re}\Big\{&\mathrm{i}\Omega\hat{H}\hat{V}_{**}^{(0)} + \frac{\mathrm{i}\Omega\hat{H}}{A_1}\Big[-\hat{V}_{\infty **}^{(10)} \\ &+ 2m\Big(\hat{\alpha}_{0**}\frac{\mathrm{d}x_0'}{\mathrm{d}y'} + (x_0'-a')\frac{\mathrm{d}\hat{\alpha}_{0**}}{\mathrm{d}y'} + \frac{\mathrm{d}\hat{z}_{0**}}{\mathrm{d}y'} - \tfrac{3}{4}c'\frac{\mathrm{d}\hat{\alpha}_{0**}}{\mathrm{d}y'}\Big) \\ &+ \hat{V}_{**}^{(0)}\Big(m(\ln\tfrac{1}{4}c'+1)\frac{\mathrm{d}c'}{\mathrm{d}y'} + 2m\frac{\mathrm{d}a'}{\mathrm{d}y'} + \kappa' c'(\tfrac{1}{4}+\tfrac{3}{2}m^2 + (m^2-\tfrac{1}{2})\ln\tfrac{1}{4}c')\Big)\end{aligned}$$

$$+mc'(\ln\tfrac{1}{4}c'+\tfrac{3}{2})\frac{\mathrm{d}\hat{V}^{(0)}_{**}}{\mathrm{d}y'}\Big]$$

$$+\mathrm{i}k'\Omega\hat{H}[-\hat{V}^{(01)}_{\infty**}-2\mathrm{i}(x'_0-a'-\tfrac{3}{4}c')\,\hat{\alpha}_{0**}$$

$$+2\mathrm{i}\,(\cos\Lambda(\tfrac{3}{4}c'+a')-\hat{z}_{0**})-\mathrm{i}c'(\ln\tfrac{1}{4}c'+\tfrac{3}{2})\,\hat{V}^{(0)}_{**}]$$

$$+2\mathrm{i}\frac{\Omega}{A_1}[(a'+\tfrac{1}{4}c')\,(\cos\Lambda+\hat{\alpha}_0)-(\hat{z}_0+\hat{\alpha}_0 x'_0)]\,\hat{V}^{(0)}_{**}\Big\}\,\mathrm{d}y'. \tag{21}$$

The thrust coefficient can be readily found by determining the wake-energy loss coefficient $\langle\mathbb{C}_E\rangle$ from an analysis of the far wake, but which may also be determined by the spanwise circulation distribution, $\hat{\Gamma}^{(0)}(y)=\cos\Lambda\,\hat{\Gamma}^{(0)}(y')$, the centreline geometry, $x=x_{\mathrm{c}}(y)$, and the reduced frequency $\Omega=kA_1$. Following some lengthy algebra, we obtain

$$\langle\mathbb{C}_E\rangle=\pi\int_{-1}^{1}\cos^3\Lambda c'\,\mathrm{Re}\{\hat{V}^{(0)}_{**}(A_1^{-1}\hat{V}^{\infty}_{(10)}+k'\hat{V}^{\infty}_{(01)})\}\,\mathrm{d}y'. \tag{22}$$

The product $\hat{V}^{(0)}_{**}\,\hat{V}^{\infty}_{(10)}$, being the quasi-steady contribution, corresponds to the induced drag in Prandtl's original theory, which results from a rotation of the local Joukowski force at the lifting line. In fact, it is identifiable with the Trefftz plane kinetic-energy loss,

$$\langle\mathbb{C}_E\rangle_{\text{Trefftz}}=-\frac{1}{2\pi A_1}\int_{-1}^{1}\hat{\Gamma}^{(0)}\left(\int_{-1}^{1}\frac{\mathrm{d}\hat{\Gamma}^{(0)}/\mathrm{d}y_1}{y_1-y}\,\mathrm{d}y_1\right)\mathrm{d}y \tag{23}$$

being independent of the centrelinc geometry. This can be proven for a straight oblique wing, and has also been verified numerically for wings with curved centrelines to within 2% in the samples: (i) $K=0.2$, $\Omega=1.5$, $A_1=10$, $x_{\mathrm{A}}=0$, $\hat{z}_{\mathrm{A}}=-\mathrm{i}\,0.78$, and $\hat{\alpha}_0=0$, (ii) $K=1$, $\Omega=1.5$, $A_1=10$, $x_{\mathrm{A}}=0.2$, $\hat{z}_{\mathrm{A}}=0$, and $\Theta=0.6$.

5. Computation of power, thrust and efficiency: preliminary remarks

Extensive computations of the lunate-tail performance were made by Chopra & Kambe (1977) for a variety of planforms, mostly in the frequency range corresponding to a relatively high $\Omega\equiv kA_1$. The mode of oscillation considered was limited to heaving and pitching about a single pitch axis corresponding to the rigid-plate mode of (6) with $\hat{\alpha}_0=\hat{z}_0=0$; a similar mode shape was assumed in the computational study by Lan (1979). Consequently, the proportional-feathering concept applies only to a limited portion of the lifting surface, close to the pitch axis. In fact, heaving of the (major) pitch axis corresponding to transverse peduncle motion is a necessary element of the motion, and a more uniform proportional-feathering distribution and together with a moderate peduncle movement may significantly enhance the performance; their effects will be investigated with the mode shape defined by (6). The effect of centreline sweep on these performance measures will also be discussed.

Propulsive efficiency is meaningful only if adequate thrust can be generated to overcome the resistance. The result of the efficiency calculation, such as η *vs.* K or η *vs.* Ω, will therefore be carried out for a few fixed values of the thrust coefficient $\langle\mathbb{C}_T\rangle$. Since $\langle\mathbb{C}_T\rangle$ is obtained as an explicit function of Θ, K, Ω, etc., maintenance of a constant $\langle\mathbb{C}_T\rangle$ implies a readjustment of Θ (or other parameters) for each different K or Ω. This is accomplished by applying the $\langle\mathbb{C}_T\rangle$ formula interactively, at a computer terminal. The values chosen for $\langle\mathbb{C}_T\rangle$ are typically 0.1, 0.3, and 0.6.

Note that the theory allows a $\langle \mathbb{C}_T \rangle$ as large as order unity. The Reynolds numbers in most examples of lunate-tail propulsion, to which the present theory [$k = O(A_1^{-1}) \ll 1$] applies, lie in the range $10^4 < Re < 10^6$ which overlaps with the upper Re range for laminar–turbulent transition (Schlichting 1979). Although few data are available for this Re range, one may nevertheless suppose that the boundary layer may still be laminar, in which case the zero-lift drag coefficient $C_{D_0} = \text{Drag}/\frac{1}{2}\rho U^2 S_w$ of the airfoil (alone) may be closely approximated by that of a laminar flat plate with $2 \times 1.33/Re^{\frac{1}{2}}$, provided boundary-layer separation does not occur upstream of the trailing edge. The realization of unseparated laminar boundary layers on well-designed airfoils has been described by Althaus (1980), where at $Re = 2 \times 10^5$, a minimum $C_D = 6 \times 10^{-3}$ corresponding to the laminar flat-plate result at the same Re is achieved for a NACA 0009 section. Moreover, a number of dynamic stall studies (see McCroskey 1982, for a review) indicate that favourable unsteady motion may allow unseparated laminar flows at Reynolds numbers considerably beyond this range. While the skin friction might increase owing to a boundary-layer thickening, such an effect cannot introduce unit-order changes in skin friction, so long as the pressure and velocity perturbations remain small.

The thrust coefficient required to overcome the parasite drag is

$$\langle \mathbb{C}_T \rangle = C_{D_0}^{(T)} \frac{S_F}{c_0 b \epsilon^2}, \tag{24}$$

where $C_{D_0}^{(T)}$ indicates the total parasite drag. Now, the ratio of the fin projected area S_F to $(c_0 b)$ is $\frac{4}{3}$ for the planform considered ((7) and (8)). Assuming (laminar) separation does not occur, and if ϵ is taken to be 0.12, the value of $\langle \mathbb{C}_T \rangle$ required to produce a thrust to just overcome the parasite drag of the lifting surface alone is 0.60 in this case. However, with an ϵ twice or triple the value of 0.12, a thrust coefficient at $\langle \mathbb{C}_T \rangle = 0.60$ will produce a thrust four or nine times the parasite drag of the fin and should suffice for propulsion and acceleration. We note that the laminar skin-friction coefficient for the body based on the wetted area is much less than that for the fin. Therefore $C_{D_0}^{(T)}/C_{D_0}$ is far less than $S^{(T)}/S_F$, where $S^{(T)}$ is the total projected area.

6. Results and discussion

6.1. *Lunate-tail performance: optimum sweep*

The first set of performance computations were made with lunate-tail models belonging to the 'feathering case' where Θ is constant (uniform spanwise), with the study of the sweep effect on the propulsive efficiency at a fixed thrust coefficient as the main objective. The data will be plotted against K which is the averaged tangent of the centreline sweep angle for the lunate shape $x_c = Ky^2$. The centreline sweep increases x_c in the function $\hat{H} \equiv x_c - x_A - \hat{z}_A$, which, in turn, determines the local heaving displacement and hence may increase the efficiency without loss of thrust, as suggested by the quasi-steady two-dimensional theory, cf. (5a, b). This performance enhancement should be most pronounced for cases involving small values of x_A and $\hat{z}_A$, implying very limited movement of the peduncle. Although a relatively large $\hat{z}_A$ is vital in the rigid case ($\hat{\alpha}_0 = \hat{z}_0 = 0$) to be studied later, the examples with small x_A and $\hat{z}_A$ will demonstrate that, with adequate sweep, a large peduncle movement is not strictly necessary. Note that with a $|\hat{z}_A|$ as large as unity, the physical dimension of the peduncle-displacement amplitude $|\hat{z}_A| = \epsilon b$ remains

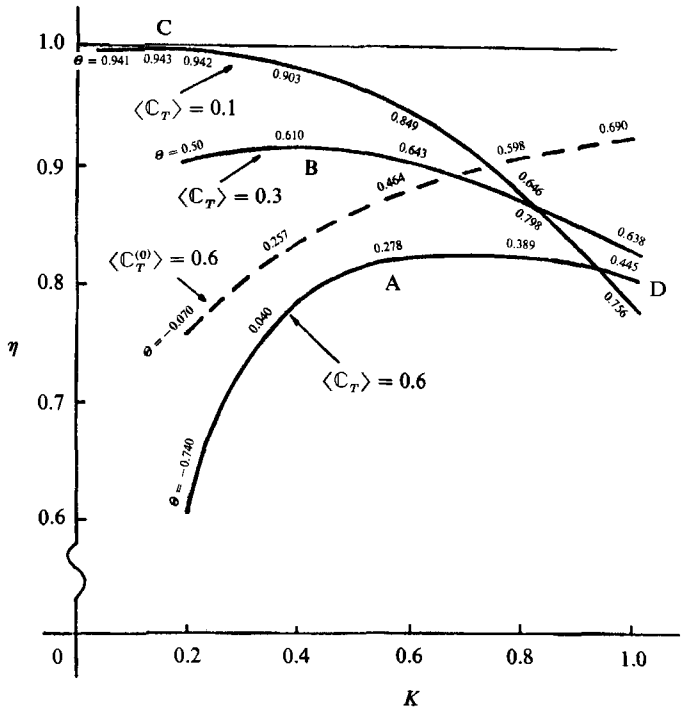

FIGURE 6. Propulsive efficiency η of parabolic lunate tail in the feathering case as a function of averaged sweep K for three thrust levels $\langle \mathbb{C}_T \rangle = 0.1$, 0.3 and 0.6; $\Omega = 1.5$, $A_1 = 10$, $x_0'/c' = 1/4$, $x_A = -0.2$, $\hat{z}_A = 0$. The proportional-feathering parameter Θ is uniform spanwise, but must be adjusted for different sweeps, K, to maintain a constant thrust coefficient $\langle \mathbb{C}_T^{(0)} \rangle = 0.6$ in the leading-order approximation.

small compared with the half-span. Figure 6 presents the results of computations for three assigned values of $\langle \mathbb{C}_T \rangle$: 0.10, 0.30, and 0.60 over the sweep range $0 < K < 1$. In this set of calculations, the aspect ratio $A_1 = 10$, the reduced frequency $\Omega \equiv kA_1 = 1.50$, and $\hat{z}_A = 0$ but $x_A = -0.2$. The local pitch axis is assumed to be at the quarter-chord line $x_0' = \frac{1}{4}c'$. The result for the set with $x_A = 0$ is similar but the performance is considerably inferior. In order to maintain the same thrust in these cases, Θ must vary with K, as noted earlier, and values of Θ are marked periodically along these curves.

The existence of an optimum sweep K depending on the thrust coefficient is clear. While the peak efficiency decreases somewhat with increasing thrust, the benefit of sweep is more noticeable at the higher $\langle \mathbb{C}_T \rangle$. For $\langle \mathbb{C}_T \rangle = 0.60$, the efficiency remains above 0.8 over a broad range $0.5 < K < 1.0$.

Figure 6 also shows the results (dashed curve) computed for $\langle \mathbb{C}_T \rangle = 0.60$ by using only the leading-order approximation (corresponding to the quasi-steady strip theory) for the thrust, i.e. $\langle \mathbb{C}_T^{(0)} \rangle \equiv 0.60$. The dashed curve gives an η-value considerably higher than the corresponding results for $\langle \mathbb{C}_T \rangle = 0.60$, and shows a trend of asymptotically increasing η with K, consistent with two-dimensional arguments noted earlier. The significant difference between the two curves not only demonstrates the importance of the three-dimensional and unsteady corrections, but also suggests that the three-dimensional corrections are responsible for reducing the thrust (at fixed Θ); this would be consistent with the observed efficiency reduction

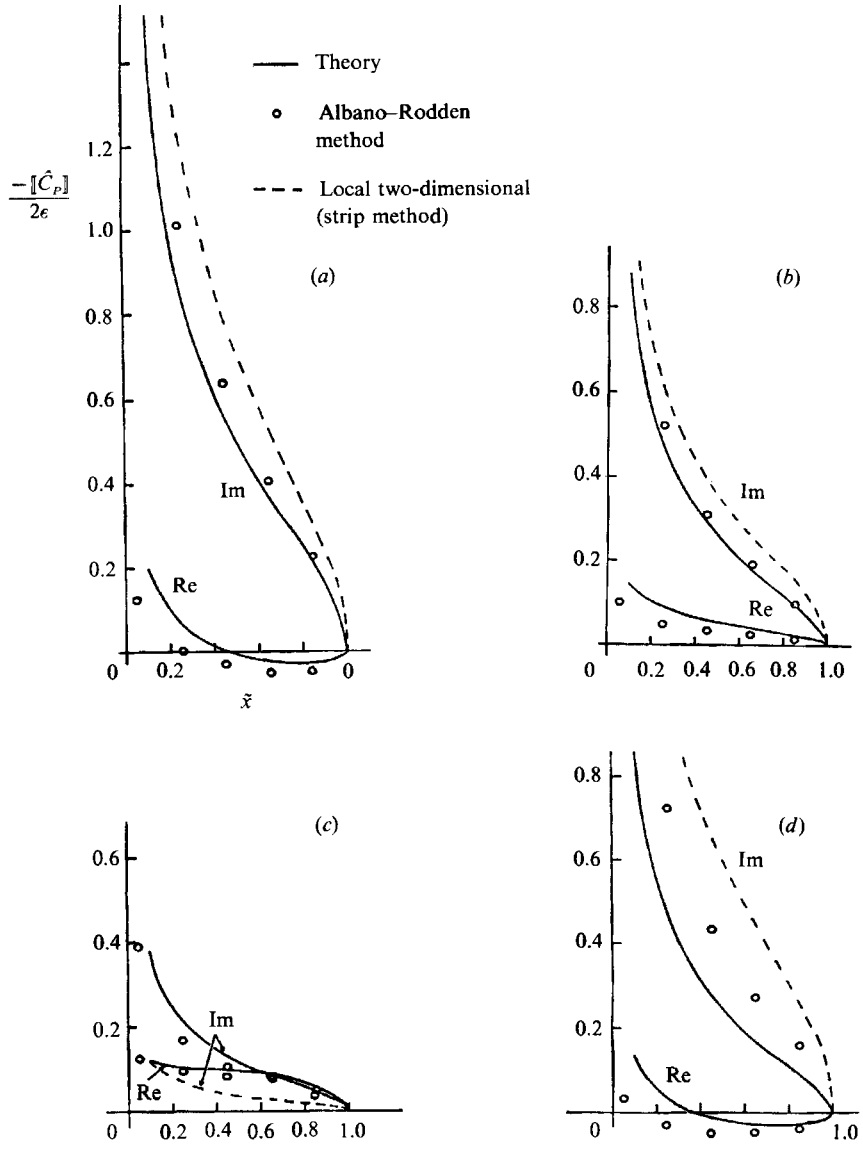

FIGURE 7. Examination of adequacy of the asymptotic theory at four conditions, (*a–d*) respectively, shown as A, B, C and D in figure 6: comparison with the doublet-lattice results of lift distributions at the same span-station, $y = 0.575$. $A_1 = 10$, $\Omega = 1.5$, $x_A = -0.2$, $\hat{z}_A = 0$. (*a*) $\Theta = 0.278$, $K = 0.6$; (*b*) $\Theta = 0.61$, $K = 0.4$; (*c*) $\Theta = 0.943$, $K = 0.1$; (*d*) $\Theta = 0.445$, $K = 1.0$.

at large K. Computation confirms that the thrust corrections are all negative, which may be used to construct a model analysis to explain the existence of a maximum η at an optimum K, at least for a small $(1-\Theta)$ and $\langle \mathbb{C}_T \rangle$ (Cheng 1989).

The existence of a minimum wake-energy loss resulting from a balance between the leading-order thrust and its three-dimensional correction shown above would suggest the breakdown of the asymptotic theory at the optimum and larger K. A comparison of the surface pressure distributions obtained in CM84 with the corresponding data from the doublet-lattice method of Albano & Rodden (1969) allows us to test the adequacy of the theory in the range of large K. This has been

FIGURE 8. (*a*) Swept wing with a V-shaped centreline. (*b*) Swept wing with a V-shaped leading edge but a curved centreline.

done for the cases corresponding to the three maxima A, B and C, as well as another case D, marked in figure 6. Representative results are given in figure 7, where the pressure coefficient is plotted against the normalized chord length. The full curve represents the theory of CM84, the open circles are the data from the doublet-lattice method and the dashed curve is from the quasi-steady two-dimensional theory. The real and imaginary parts of the pressure coefficient are designated by Re and Im respectively. Only the surface pressure distributions at the 57.5% span station are shown in each case. Despite the relatively large corrections for the A, B and C cases, the agreement with the doublet-lattice method is surprisingly good. In case D where the three-dimensional correction at $K = 1$ is clearly excessive (figure 6), the asymptotic theory is apparently in need of improvement and this aspect will be discussed later. In any event, the magnitude and solution behaviour given by the theory in figure 7 for case D may still represent an improvement over the quasi-steady two-dimensional result.

6.2. *Problems with V-shape tails; the importance of peduncle movement*

We wish to compare the performance of a parabolic-shaped lunate tail to that of the V-shaped tail to determine the influence of the centreline curvature. However, a V-shaped centreline has an excessive, singular downwash at the apex, induced mainly by the bound vortex on the opposite side of the fin panel (figure 8*a*). This feature of the lifting-line theory has been discussed also by Cheng *et al.* (1981) in steady compressible flow and is believed to be the cause for the 'middle effect' of a flying wing aircraft (Horton & Selinger 1983). This excess downwash would cause an irregularity in the span load and on the flow, requiring the use of a higher real camber or a higher incidence at the wing root, as is evident from most modern swept-wing transport aircraft. Apart from its aerodynamic drawbacks, the downwash singularity also causes a local breakdown of the asymptotic theory. Here, we resolve the problem with a vanishing span load at the apex, i.e. $\hat{\Gamma}^{(0)} = 0$ at $y = 0$, which amounts to requiring that $x_A = \hat{z}_A = 0$ (a frozen peduncle), or more generally $(x_A + \hat{z}_A) = 0$ for the V-shaped centreline $x_c = m_0|y|$.

Note that the centreline of a planform with a pair of straight, swept leading edges is not necessarily of V-shape (see figure 8*b*). Many species in the order percomorphi with lunate tails appear to possess similar trailing-edge contours.

To provide a fair comparison of results with the two dissimilar centreline shapes, we first compare the V-shape with a parabolic shape having the same tip and major pitching axis locations as illustrated in figure 9(*a*). This is equivalent to a parabolic shape with $K = m_0 + x_A$, chosen so as to round-off the apex of the V-shape centreline.

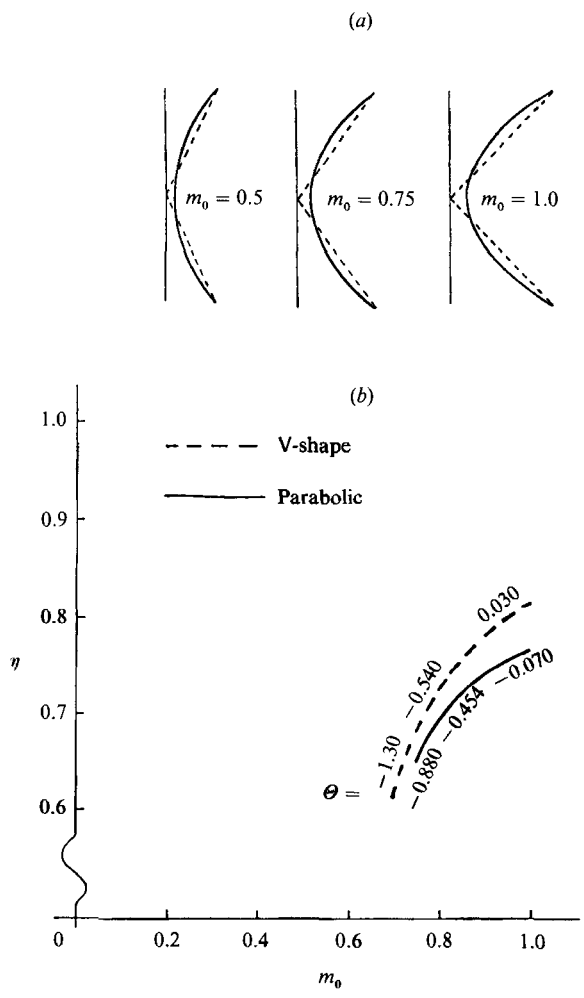

FIGURE 9. Comparison of parabolic lunate and V-shaped centrelines in the feathering case: (*b*) propulsive efficiency *vs.* a sweep parameter m_0 at a fixed thrust coefficient $\langle \mathbb{C}_T \rangle = 0.60$, $\Omega = 1.0$, $A_1 = 10$, $x_0'/c' = \frac{1}{4}$, and $\hat{z}_0 = 0$. m_0 is the tangent of the sweep angle of the V-shaped centreline; the corresponding parabolic centreline is shown in (*a*) for three values of m_0. Note that the tail tips coincide but the major pitch axis locations differ.

The set of parabolic lunate planforms in figure 9(*a*) assumes an m_0 dependence as $x_A = -\frac{1}{6}m_0$. The results of these two families are presented in figure 9(*b*) as the efficiency η *vs.* the sweep parameter m_0 for the specified thrust coefficient $\langle \mathbb{C}_T \rangle = 0.60$, for aspect ratio $A_1 = 10$ at the reduced frequency $\Omega = 1.0$, with $\hat{z}_0 = 0$, $x_0' = \frac{1}{4}c'$. The values of Θ required to maintain the specified thrust level are marked at successive points along the curves. On account of the rather high thrust level considered, the Θ-values turn out to be far from unity. Note that no heaving of the major pitch axis is allowed for the parabolic lunate tail ($\hat{z}_A = 0$). The V-shaped fin results (dash curve) are apparently superior to the parabolic shape (solid curve) for the same m_0 and promise high performance in the high sweep range $m_0 > 1$. On the other hand, if the differences in the x_A values of the parabolic family are ignored (x_A is -0.128 and -0.167 at $m_0 = 0.7$ and 1, respectively), converting the curve η *vs.* m_0 to η *vs.* K should shift the parabolic lunate result reasonably close to the case with $x_A = -0.20$ shown

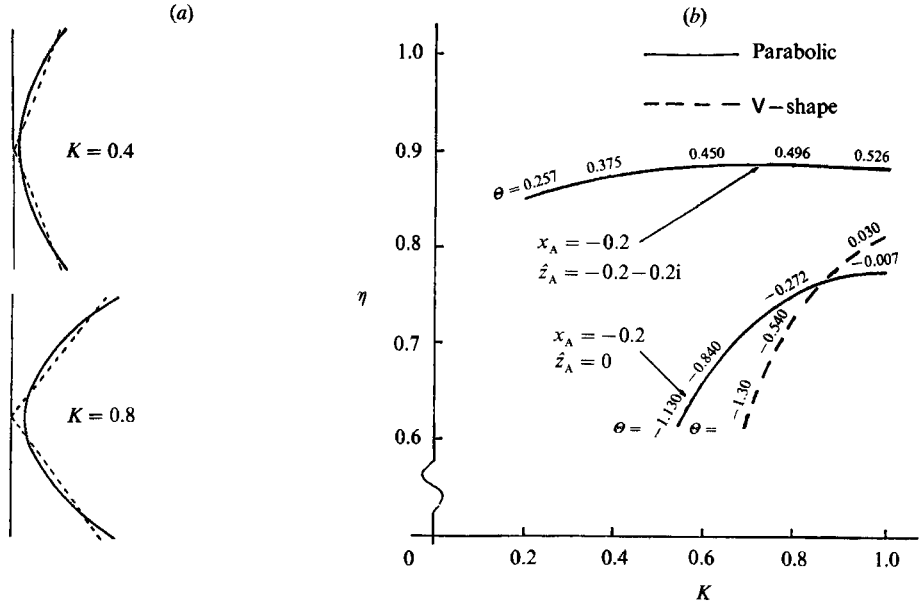

FIGURE 10. Comparison of parabolic and V-shaped centrelines in the feathering case: (*b*) propulsive efficiency *vs.* the average tangent of the sweep angle K at a fixed thrust $\langle \mathbb{C}_T \rangle = 0.60$, $\Omega = 1.0$, $A_1 = 10$, $x_0'/c' = \frac{1}{4}$, and $\hat{z}_0 = 0$. Note improvement in performance by allowing small changes in the major pitch-axis location and its heaving displacement, x_A and $\hat{z}_A$.

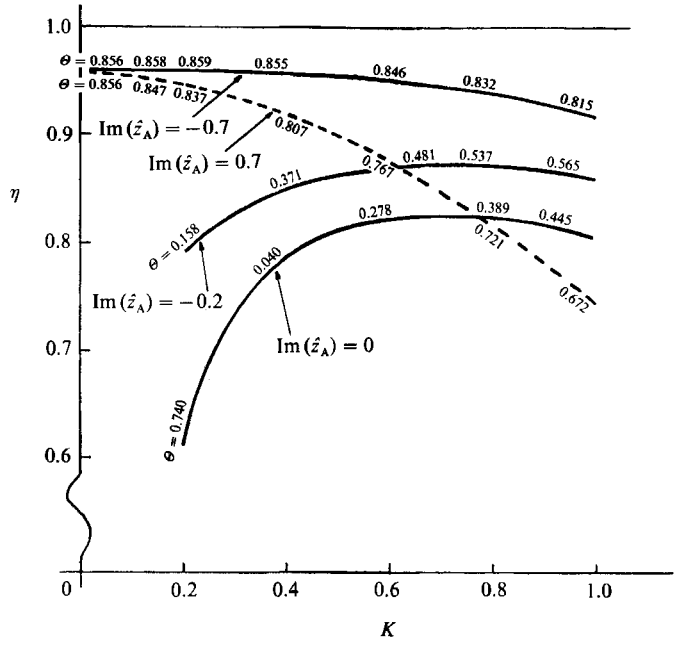

FIGURE 11. Performance enhancement of parabolic lunate tails through properly tuned peduncle movement in the feathering case: η *vs.* K at fixed $\langle \mathbb{C}_T \rangle = 0.6$ for four imaginary values of $\hat{z}_A$ and $\mathrm{Re}(\hat{z}_A) = 0$; $\Omega = 1.5$, $A_1 = 10$, $x_A = -0.2$. Note, with a higher $\mathrm{Im}(\hat{z}_A)$, performance benefit of sweep becomes less apparent.

earlier. This suggests the alternative comparison shown in figures 10(*a*) and 10(*b*), in which the two results (dashed and lower solid curves) are compared as η *vs.* K, with K now taken to be the averaged tangent of the sweep angle, assuming $x_A = -0.20$, $\hat{z}_A = 0$ for the parabolic case. Note that in this comparison, the fin tips of the two families no longer coincide. Thus an evolution from the V-shape to the parabolic centreline, with a pitch axis located slightly anterior to the tail, may result in a performance enhancement in the moderate sweep and frequency domain $K \sim 0.70$ and $\Omega \sim 1$.

The location $x_A = -0.2$ in the parabolic case (solid curve) is equivalent to a peduncle heaving displacement with $\mathrm{Re}\,(\hat{z}_A) = -0.2$, and thus favourable effect of peduncle movement suggests that a still more effective enhancement might be achieved with the deployment of both parts of $\hat{z}_A$. The result of setting $\hat{z}_A = -0.2(1+i)$ in addition to $x_A = -0.2$ is presented as the upper solid curve in figure 10(*b*). This enhancement with a relatively small peduncle movement is not entirely unexpected, if one recalls the dependence of $\langle \mathbb{C}_T \rangle$ on $|\hat{H}|^2$ and the manner in which x_A and $\hat{z}_A$ affect $\hat{H}$ (equations (9), (19)). We also note that the efficiency curves in figures 9(*b*) and 10(*b*) are generally lower than those in figure 6, which were computed for a higher reduced frequency ($\Omega = 1.50$).

To ascertain the significant influence of the peduncle displacement $\hat{z}_A$ on a lunate tail, we present the results with $\mathrm{Im}\,(\hat{z}_A) = \pm 0.70$ in figure 11 where results with $\mathrm{Im}\,(\hat{z}_A) = 0$ and -0.2 are also shown. The performance enhancement through $\mathrm{Im}\,(\hat{z}_A)$ is indeed large. Apparently, with the relatively large value of $|\hat{z}_A| = 0.70$, the optimum sweep is so small that practically any sweep ($K > 0$) tends to reduce the efficiency. In this instance, η is rather high ($\eta = 0.90$–0.95) for moderate sweep ($K < 0.50$), and the case with a negative $\mathrm{Im}\,(\hat{z}_A)$ is superior in maintaining $\eta > 0.90$ for all $K < 1.0$.

In order to maintain high propulsive efficiencies, the development of a V-shaped tail should be accompanied by reduced peduncle motion (or its equivalent: $x_A + \hat{z}_A = 0$) and increased sweep angles. The condition $x_A + \hat{z}_A = 0$ implies either a zero phase lag for $x_A < 0$, or a 180° phase lag for $x_A > 0$ for the peduncle motion of a V-shaped fin. It remains to be seen whether this is true of real life. Also, according to this performance analysis, the reduced sweep of a parabolic lunate tail may be compensated for by an increased amplitude of peduncle motion; conversely, increased sweep angles enable high efficiencies to be maintained in the presence of constraints on the peduncle motion.

6.3. *Comparisons with the rigid-plate oscillation*

Figures 8, 9, and 11 assume that the peduncle movement is not restricted by physiological or structural constraints. If $\hat{z}_A = O(1)$, i.e. $z_w = O(\epsilon b)$ at $x = x_A$, is permitted, even a rigid plate, in heaving and pitching about a single axis, may perform impressively with appropriate tuning of the relative phase and pitch-axis location. The proportional-feathering concept may still be useful in this case, but is relevant only over the fin area close to the pitch axis $x = x_A$ (figure 12). Proportional-feathering control will clearly depend on the centreline sweep and the pitch-axis location; thus for $x_A = 0$, proportional feathering applies more effectively to an unswept fin than to one with $K \neq 0$. For $x_A > 0$, on the other hand, performance may be enhanced by the sweep.

With $\hat{\alpha}_0 = \hat{z}_0 = 0$ in this rigid case, the functions $\hat{H}$ and Θ become

$$\hat{H} = x_c - x_A - \hat{z}_A, \quad \Theta = \frac{\mathrm{i}}{\Omega \hat{H}}. \tag{25}$$

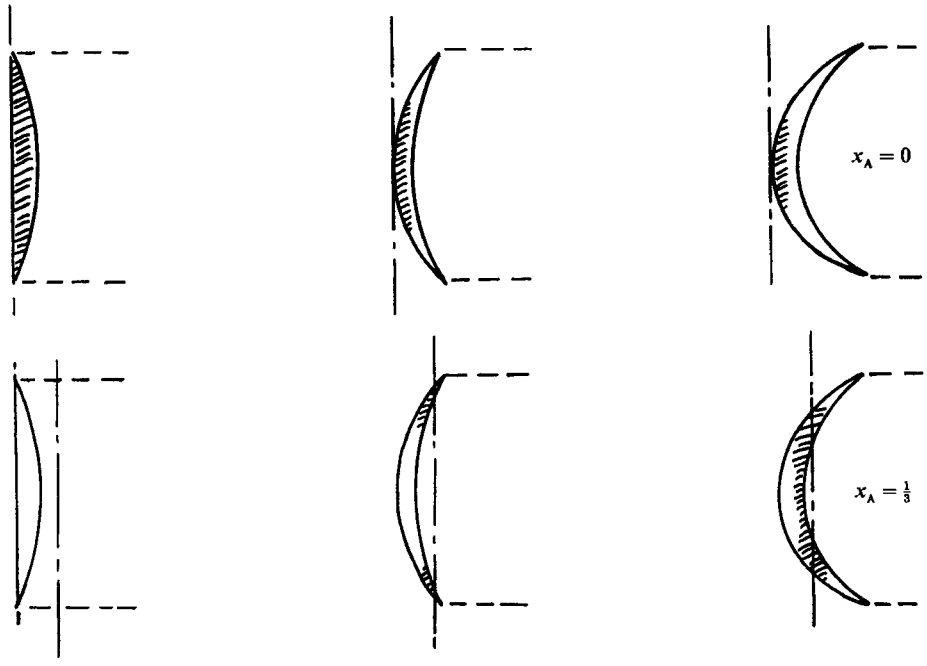

FIGURE 12. Illustration of regions on lunate tails in rigid-plate mode (shaded areas) over which concept of proportional feathering remains applicable. Extent of the (shaded) region depends on pitch-axis location and planform.

Note that $\hat{H}$ and Θ are both necessarily non-uniform spanwise here. At the pitch axis ($x = x_A$), the proportional-feathering parameter is $\Theta = \Theta_L \equiv -i/\Omega\hat{z}_A$. Therefore,

$$\mathrm{Re}\,(\Theta) = \mathrm{Re}\,(\Theta_L) = -1/(\Omega\,\mathrm{Im}\,(\hat{z}_A)). \tag{26}$$

From two-dimensional analysis, Lighthill (1970) showed that Re (θ) must be positive and less than one for thrust generation. Consequently, in (26) Im ($\hat{z}_A$) is negative, and the peduncle movement must lag behind that of the pitch of the rigid fin. Efficient propulsion can be achieved in this case only if $\hat{z}_A$ can be brought sufficiently close to $-i/\Omega$. If the peduncle were frozen (i.e. if $\hat{z}_A \equiv 0$), Θ becomes $i/\Omega(x_c - x_A)$ and would be far from unity, when propulsion is not expected to be efficient.

Figure 13 presents the results of a performance analysis for the family of oscillating rigid lunate plates with $x_c = Ky^2, A_1 = 10$ at reduced frequency $\Omega = 1.50$, allowing Im ($\hat{z}_A$) $\neq 0$. To make a meaningful comparison with one of the feathering cases considered earlier in figure 11, the results are plotted as curves of η *vs.* K for the fixed thrust coefficient $\langle C_T \rangle = 0.60$. We take Re ($\hat{z}_A$) = 0, since the latter can be absorbed into the axis location x_A. Four curves corresponding to four different axis locations, $x_A = -0.2$, 0, 0.15 and 0.30, are shown. The only remaining mode-shape parameter is Im ($\hat{z}_A$) which is adjusted to maintain $\langle C_T \rangle = 0.60$ as K changes. These required values of Im ($\hat{z}_A$) are marked along the curves. Except when $x_A < 0$, there exists an optimum value of K which increases with x_A, from $K = 0$ for $x_A = 0$ to $K = 0.6$ for $x_A = 0.30$. This is consistent with the observations made in figure 12. The efficiency, η, reaches 0.95 at $x_A = 0$, while Im ($\hat{z}_A$) varies from -0.617 to -0.79. Here, the values $-1/(\Omega\,\mathrm{Im}\,(\hat{z}_A))$ are indeed close to unity, as may be expected for a high efficiency. The peak efficiency, 0.95 in this case, is only slightly lower than that of the corresponding curve in figure 11 for the feathering case at the same $\langle C_T \rangle = 0.60$,

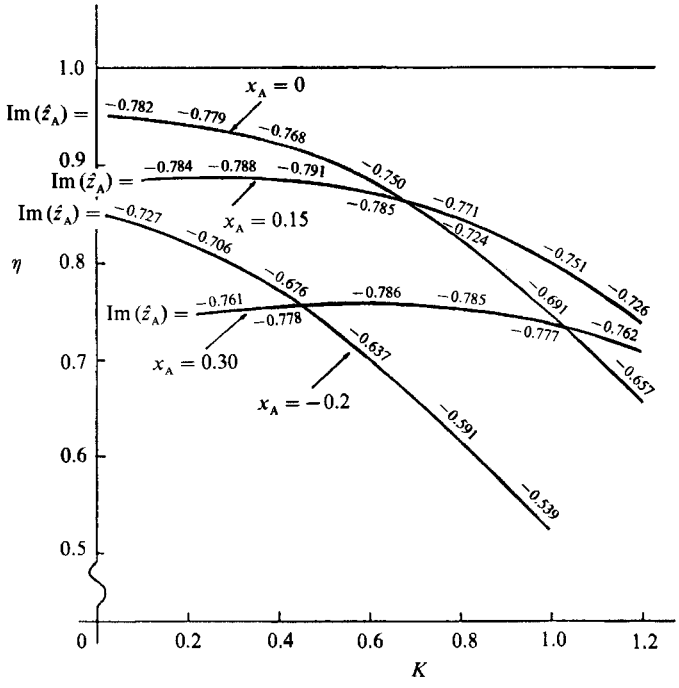

FIGURE 13. Propulsive efficiency of parabolic lunate tail in the rigid-plate mode as functions of the averaged sweep parameter K at a fixed thrust $\langle \mathbb{C}_T \rangle = 0.60$ for four different pitch-axis locations: $\Omega = 1.5$, $A_1 = 10$, and $\mathrm{Re}\,(\hat{z}_A) = 0$. Note that the imaginary part of the $\hat{z}_A$ in this case must be adjusted for each K to maintain a constant thrust.

although the η in figure 11 with comparable Im $(\hat{z}_A)$ deteriorates with large K at a much lower rate and η is considerably higher for K away from $K = 0$.

The foregoing analysis confirms the apparently interchangeable roles of sweep and peduncle movement in providing adequate heaving displacement at each local span station so as to reduce the value, or the averaged value, of $(1-\Theta)$. When a sizeable transverse displacement at the peduncle of the order (ϵb) is allowed, and properly tuned, the sweep is no longer required and, for a rigid fin, sweep even causes a deterioration in performance. If, on the other hand, additional constraints favour a stiffer posterior body movement, hence a smaller Im $(\hat{z}_A)$, the sweep can be used to augment the heaving action at the local span stations. This can be realized with the help of additional pitching about a local curved axis. The feathering case considered here is but one of such examples; comparable results may be realized in nature by passive structural response. Note that our feathering case with a spanwise uniform Θ is not the result of an optimum three-dimensional analysis. It is for these feathering cases with a constricted peduncle movement (small Im $(\hat{z}_A)$) that the sweep is seen to play a beneficial role. It may be added that the performance of a flexible lunate tail may be enhanced further by relaxing values of x_A or Re $(\hat{z}_A)$ to the negative range of the unit order.

The results in figure 13 are in qualitative agreement with the earlier study of Chopra & Kambe (1977), which treated only mode shapes corresponding to the rigid cases at high reduced frequencies. Yates (1983) has compared the numerical model results of Chopra & Kambe (1977) using experimentally determined morphological and kinematic data for porpoise (*Lagenoryncus obliquidens*) and kawakawa

(*Euthynnus affinis*), and has noted that the calculated values of thrust and efficiency were likely to be upper bounds, and this observation is well supported by the results presented here. There remains a need for more precise field data before an independent evaluation of some of the more detailed model predictions may be attempted.

7. Discussion and conclusions

The present study underlines the importance of three-dimensional and unsteady corrections to the earlier two-dimensional results (Lighthill 1969, 1970). The two-dimensional theory neglects the trailing vortices which represent a major portion of the vortex wake in the frequency domain considered, and hence yields a higher propulsive efficiency.

The importance of the parameter Θ, representing a generalization of Lighthill's proportional-feathering parameter, is identified, and the sweep and curvature effects of the centreline on the propulsive efficiency of a lunate-tail planform have been ascertained. In the feathering case, where the local pitching angle varies along the span in a special way, an optimum sweep can be obtained at each thrust level (and for each peduncle displacement amplitude) by varying the proportional-feathering parameter. The corresponding optimum efficiency may be further enhanced by moderately increasing the heaving amplitude of the major pitch axis (peduncle) as long as the assumption of small perturbations remains adequate. However, an increase in the heaving amplitude of the peduncle decreases the value of the optimum sweep until the latter becomes zero. Using the results obtained for a V-shaped centreline (zero curvature) with a frozen peduncle or its equivalent ($x_A + \hat{z}_A = 0$) as a baseline, the propulsive efficiency generally improves with centreline curvature, and this improvement is further enhanced in cases involving peduncle motion.

In the rigid case, where the local pitching angle $\hat{\alpha}_0 = 0$, the propulsive efficiency is high for an unswept fin and quickly deteriorates with increased sweep, at a rate higher than that for the feathering case.

Certain biological implications and interpretations of this performance analysis may be advanced, whilst still leaving in mind the restricted domain of the asymptotic analysis. If one postulates a tendency in carangiform evolution towards increasingly restricted motion of the caudal peduncle, in the interests of reducing wake-energy losses, for example, then the increase in sweep angle of the tail appears as a design option to compensate for the reduced peduncle heaving amplitude. However, a simple swept-back arrangement such as a V-shaped centreline carries with it a penalty of excessive upwash at the centreline (in the symmetry plane), unwelcome both in practical and analytical terms. This may be avoided either by unloading the wing at the centreline, or by rounding off the apex of the V here. The latter option will modify the V-shaped wing/tail towards the characteristic crescent-moon shape of the lunate tail. Alternatively, the frozen peduncle condition (equivalently, $x_A + \hat{z}_A = 0$) permits a V-shaped centreline, provided that the sweep angle is sufficient ($m_0 \geqslant 1$) to maintain reasonable propulsive efficiencies without loss of thrust. Although non-negligible lateral peduncle motion may be observed in V-shaped-tailed fish (e.g. Webb 1975), sufficient data are not yet available to determine whether adherence to the condition $x_A + \hat{z}_A = 0$ is indeed (inversely) correlated with centreline curvature. It should be noted that large-amplitude tail motion found in nature may exceed the range of the present asymptotic theory, which can treat with confidence only a relatively small transverse displacement, i.e. $z_w = O(\epsilon b) = O(c_0)$.

However, according to theoretical and experimental two-dimensional studies (Chopra 1976; Katz & Weihs 1978; Oshima & Natsume 1980), the magnitude of corrections needed for large amplitudes in the frequency domain of interest appears to be rather limited. A systematic nonlinear correction to the linear theory might thus be able to account for the finite-ϵ effect.

Further useful parametric studies remain, particularly with regard to the peduncle displacement $\hat{z}_A$, the centreline geometry $x_c(y)$, the distribution of the proportional feathering $\Theta(y')$, and their optimization with various constraints. More extensive studies on the rigid-plate mode, which promises an impressive performance with relatively simple kinematic and structural requirements, are of great interest. Equally and perhaps more important is to ascertain whether the performance of a flexible lunate tail may be enhanced by the further tuning of the peduncle motion $\hat{z}_A$, and at higher thrust coefficients.

The analysis may be extended to ornithopter mode propulsion following a relatively simple modification of the mode in (6) to include wing flapping, in which case a comparison with the experimental data of Archer, Sapuppo & Betteridge (1979) and with the unsteady lifting-line model of Phlips, East & Pratt (1981) would be of interest. A preliminary investigation (Cheng 1989) for the case of a straight, unswept centreline indicates that significant performance enhancement due to unsteady effects may be realized, compared with an equivalent quasi-steady analysis, such as that of Jones (1980).

This study was supported by the National Science Foundation, Contract No. CME-7926003. Partial support by the Office of Naval Research under Grant No. N00014-75-C-0520 is also gratefully acknowledged. The authors are most grateful to Ms Ellen Rae Donner and Ms Kerry Joan McKinney for typing the manuscript.

REFERENCES

Albano, E. & Rodden, W. P. 1969 A doublet-lattice method for calculating lift distributions on oscillating surfaces in subsonic flows. *AIAA J.* **7**, 279–285.

Althaus, D. 1980 *Profilpolaren für den Modelflug, Winkanal messungen Kritischen Reynolds-zahlbereich.* Neckar-Verlag, vs-Villinger.

Archer, R. D., Sapuppo, J. & Betteridge, D. S. 1979 Propulsion characteristics of flapping wings. *Aeronaut. J.* **83**, 355–371.

Ashenberg, J. & Weihs, D. 1984 Minimum induced drag of wings with curved planform. *J. Aircraft* **21**, 89–91.

Cheng, H. K. 1976 On lifting-line theory in unsteady aerodynamics. *University of Southern California, Dept Aerospace Engng Rep.* USCAE 133.

Cheng, H. K. 1989 Lifting-line theory and performance study of lunate-tail swimming and ornithopter propulsion. *University of Southern California, Dept Aerospace Engng Rep.* USCAE 150.

Cheng, H. K., Meng, S. Y., Chow, R. & Smith, R. 1981 Transonic swept wings studied by the lifting-line theory. *AIAA J.* **19**, 961–968.

Cheng, H. K. & Murillo, L. 1982 Lunate-tail swimming propulsion as a problem of curved lifting line in unsteady flow. Part 1. Asymptotic theory. *University of Southern California, Dept Aerospace Engng Rep.* USCAE 139 (referred to as CM82).

Cheng, H. K. & Murillo, L. 1984 Lunate-tail swimming propulsion as a problem of curved lifting line in unsteady flow. Part 1. Asymptotic theory. *J. Fluid Mech.* **143**, 327–350 (referred to as CM84).

Chopra, M. G. 1974 Hydromechanics of lunate-tail swimming propulsion. *J. Fluid Mech.* **64**, 375–391.

CHOPRA, M. G. 1976 Large amplitude lunate-tail theory of fish locomotion. *J. Fluid Mech.* **74**, 161–182.

CHOPRA, M. G. & KAMBE, T. 1977 Hydromechanics of lunate-tail swimming propulsion. Part 2. *J. Fluid Mech.* **79**, 49–69.

DAM, C. P. VAN 1987 Efficiency characteristics of crescent-shaped wings and caudal fins. *Nature* **325**, 435–437.

HORTON, R. VON & SELINGER, P. F. 1983 *Nuflügel*. Graz: H. Weishaupf.

JAMES, E. C. 1975 Lifting line theory for an unsteady wing as a singular perturbation problem. *J. Fluid Mech.* **70**, 735–771.

JONES, R. T. 1980 *Aero. J. R. Aero. Soc.* July, 214–217.

JOSEPH, J., KLAWE, W. & MURPHY, P. 1979 *Tuna and Billfish*. La Jolla: Inter-American Tropical Tuna Commission.

KATZ, J. & WEIHS, D. 1978 Hydrodynamic propulsion by large amplitude oscillation of an airfoil with chordwise flexibility. *J. Fluid Mech.* **88**, 485–497.

KRAMER, M. O. 1960 Boundary layer stabilization by distributed damping. *J. Am. Soc. Naval Engrs* **72**, 25–34.

LAN, C. E. 1979 The unsteady quazi-vortex-lattice method with applications to animal propulsion. *J. Fluid Mech.* **93**, 747–765.

LIGHTHILL, M. J. 1969 Hydromechanics of aquatic animal propulsion. *Ann. Rev. Fluid Mech.* **1**, 413–446.

LIGHTHILL, M. J. 1970 Aquatic animal propulsion of high hydromechanical efficiency. *J. Fluid Mech.* **44**, 265–301.

MCCROSKEY, W. J. 1982 Unsteady airfoils. *Ann. Rev. Fluid Mech.* **14**, 285–311.

MURILLO, L. E. 1979 Hydromechanical performance of lunate-tails analyzed as a lifting-line problem in unsteady flow. Dissertation, University of Southern California.

NORMAN, J. R. & FRASER, F. C. 1937 *Giant Fishes, Whales and Dolphins*. London: Putnam.

OSHIMA, Y. & NATSUME, A. 1980 Flow field around an oscillating airfoil. *Tokyo University Aerospace Research Institute Rep.* 16, No. 1A.

PHLIPS, P. J., EAST, R. A. & PRATT, N. H. 1981 An unsteady lifting-line theory of flapping wings with application to the forward flight of birds. *J. Fluid Mech.* **112**, 97–125.

PRANDTL, L. 1918 *Nachr. Ges. Wiss. Gött. Math.-Phys. Klass.*, 451–477.

SCHLICHTING, H. 1979 *Boundary Layer Theory*, pp. 452–456. McGraw-Hill.

VAN DYKE, M. D. 1964 *Perturbation Methods in Fluid Mechanics*. Academic. (see also 1975 edition, Parabolic Press).

WEBB, P. W. 1975 Hydrodynamics and Energetics of Fish Propulsion. *Bull. Fish. Res. Bd. Canada* **190**, 1–158.

WU, T. Y. T. 1971*a* Hydromechanics of swimming propulsion. Part 2. Some optimum shape problems. *J. Fluid Mech.* **46**, 521–544.

WU, T. Y. T. 1971 *b* Hydromechanics of swimming propulsion. Part 3. Swimming and optimum movements of slender fish with side fins. *J. Fluid Mech.* **46**, 545–568.

WU, T. Y. T. & YATES, G. T. 1978 A comparative mechano-physiological study of fish locomotion with implication with tuna-like swimming mode. In *The Physiological Ecology of Tunas* (ed. G. D. Sharp & A. E. Dizon), pp. 313–337. Academic.

YATES, G. T. 1983 Hydromechanics of body and caudal fin propulsion. In *Fish Biomechanics* (ed. P. W. Webb & D. Weihs), pp. 177–213. Praeger Scientific.